

## Reliability-based design of prestressed concrete girders in integral Abutment Bridges for thermal effects

WooSeok Kim<sup>1a</sup>, Jeffrey A. Laman<sup>2b</sup> and Jong Yil Park<sup>\*3</sup>

<sup>1</sup>Civil Engineering, Chungnam National University, Deajeon, 305-764, Korea

<sup>2</sup>Civil and Environmental Engineering, Pennsylvania State University, University Park, PA, 16802, USA

<sup>3</sup>Safety Engineering, Seoul National University of Science and Technology, 139-743, Seoul, Korea

(Received April 17, 2013, Revised March 11, 2014, Accepted March 20, 2014)

**Abstract.** Reliability-based design limit states and associated partial load factors provide a consistent level of design safety across bridge types and members. However, limit states in the current AASHTO LRFD have not been developed explicitly for the situation encountered by integral abutment bridges (IABs) that have unique boundary conditions and loads with inherent uncertainties. Therefore, new reliability-based limit states for IABs considering the variability of the abutment support conditions and thermal loading must be developed to achieve IAB designs that achieve the same safety level as other bridge designs. Prestressed concrete girder bridges are considered in this study and are subjected to concrete time-dependent effects (creep and shrinkage), backfill pressure, temperature fluctuation and temperature gradient. Based on the previously established database for bridge loads and resistances, reliability analyses are performed. The IAB limit states proposed herein are intended to supplement current AASHTO LRFD limit states as specified in AASHTO LRFD Table 3.4.1-1.

**Keywords:** structural reliability; bridge design; integral abutment; AASHTO, LRFD

---

### 1. Introduction

Integral abutment bridges (IABs) have become a preferred new bridge construction over the last two decades due to many advantages originating from removing expansion joints (Arockiasamy *et al.* 2004). However, IAB behavior is generally difficult to predict, prohibiting the use of conventional bridge analysis methods due to complex boundary conditions, uncertainties and nonlinearities related to ambient temperature changes, soil-structure interaction, and concrete creep and shrinkage – a much more complex condition than for jointed bridges because these thermal loads are secondary loads in jointed bridge but main loads in integral abutment bridges. Nevertheless, current IAB design practice utilizes limit states by AASHTO Load and Resistance Factor Design Bridge Design Specifications (AASHTO LRFD 2010) established for conventional jointed bridge design. Although, significant load effects experienced in IABs as a result of

---

\*Corresponding author, Assistant Professor, E-mail: [jip111@seoultech.ac.kr](mailto:jip111@seoultech.ac.kr)

<sup>a</sup>Assistant Professor, E-mail: [wooseok@cnu.ac.kr](mailto:wooseok@cnu.ac.kr)

<sup>b</sup>Professor, E-mail: [jlaman@psu.edu](mailto:jlaman@psu.edu)

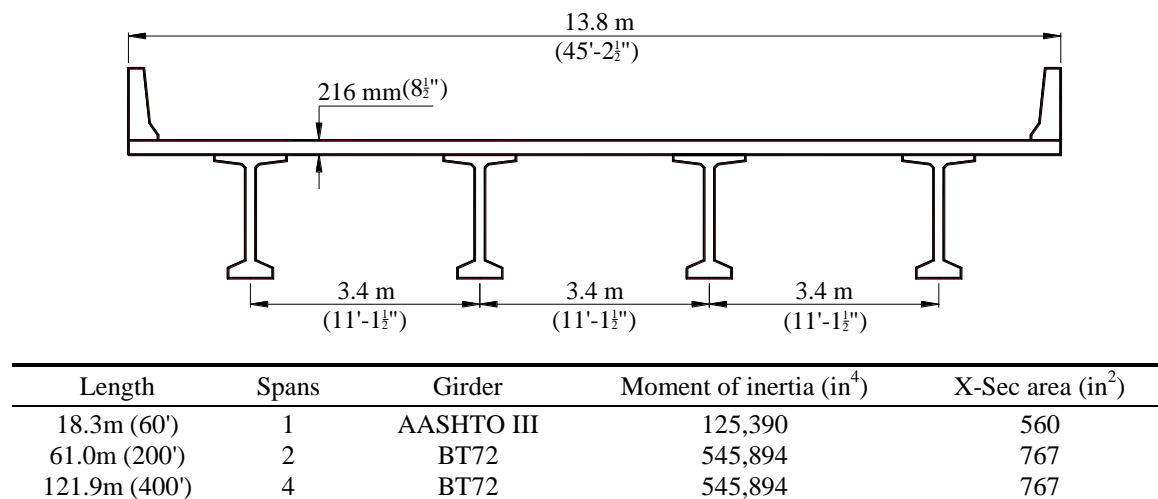


Fig. 1 Typical cross section and bridge dimensions for parametric study

horizontal earth pressure (EH), temperature gradient (TG), creep (CR), shrinkage (SH) and uniform temperature (TU), defined in AASHTO LRFD (2010), cannot be directly adopted for IAB design process because of different boundary conditions. The present study, therefore, intends to propose additional limit states for IABs supplemental to the current AASHTO LRFD limit states.

This study developed new limit states for three limit states equivalent to AASHTO LRFD limit state: Strength I, Service I and Service III. The proposed limit states used the same format as those of the current AASHTO LRFD specifications covering four prestressed concrete girder highway IABs with short to medium lengths. The typical section considered in the present study is presented in Fig. 1 (Kim and Laman 2010a). Wind loads on structures (WS) were ignorable to determine girder moment capacity in this length range of girder bridges. Based on a previous long-term field monitoring study (Kim and Laman 2012), axial forces that might exist in a girder were not considered for girder bending capacity.

The typical controlling AASHTO LRFD limit states for prestressed concrete girder jointed bridge design are as follows

$$\text{Strength I: } 1.25\text{DC} + 1.5\text{DW} + 1.75(\text{LL} + \text{IM}) \quad (1a)$$

$$\text{Service I: } 1.0\text{DC} + 1.0\text{DW} + 1.0(\text{LL} + \text{IM}) \quad (1b)$$

$$\text{Service III: } 1.0\text{DC} + 1.0\text{DW} + 0.8(\text{LL} + \text{IM}) \quad (1c)$$

The above limit states consider bridge component dead load (DC), wearing surface dead load (DW), traffic live load (LL), and vehicular dynamic load allowance (IM). AASHTO LRFD (2010) also specifies EH, TU, TG, CR and SH. For the Strength I limit state, the load factor for TG is taken as 0.0 for TU, CR and SH as 0.5 or 1.0, and for EH as 1.50 or 0.9 for the active condition, 1.35 or 0.9 for the at-rest condition and not given for the passive condition. For the Service I combination, all load factors are 1.0 except TU is either 1.00 or 1.20, and TG is taken as 0.5 when the live load is considered or 1.0 when live load is not considered. The load factors for the Service III combination is the same as Service I except that the LL factor is 0.8. Current practice uses the same limit states above for IABs, i.e., EH, TU, TG, CR and SH are considered as secondary,

Table 1 IAB response prediction models (Kim and Laman 2010b)

Bridge Bending Moment at Midspan (kN-m)	(+)	$93\alpha - 850H + 940P - 19 \geq 0$ $180\alpha + 160H + 330P - 4700 \geq 0$ $45\alpha + 1000P - 3500 \geq 0$	for $L \leq 39.7$ m for $39.7 \leq L \leq 91.5$ m for $L \geq 91.5$ m
	(-)	$-162\alpha^{0.35}L^{0.60}P^{0.20}$ $-460\alpha^{0.40}L^{0.35}$ $-4950\alpha^{0.1}P^{-0.40}$	for $H \leq 3.8$ m for $3.8 \leq H \leq 5.4$ m for $H \geq 5.4$ m

$\alpha$ : thermal expansion coefficient ( $\times 10^6$  mm/mm/°C)  
 $H$ : backfill height (m)  
 $L$ : bridge length (m)  
 $P$ : soil-pile stiffness (1=low, 2=intermediate, 3=high)

Table 2 Dead and live load statistics

Load	Distribution	Bias Factor	COV
Dead Load (Factory-made)	Normal	1.03	0.08
Dead Load (Cast-in-place)	Normal	1.05	0.10
Dead Load (Asphalt Wearing Surface)	Normal	1.00	0.25
Prestressing Force ( $f_{ps}$ )	Normal	1.04	0.025
Live Load and Dynamic Load (HL-93)	Normal	1.10	0.18

independent load effects even though these are primary loads in IAB design. Instead of the commonly applied limit states of Eq. (1) to determine factored girder bending for IABs, the present study establishes additional limit states to be used for IABs by adding thermal loading terms that include EH, TU, TG, CR and SH.

To determine factored effects in the present study, all girder load effects due to EH, TU, TG, CR and SH are considered for the proposed supplementary IAB limit states and are represented by a single thermal loading term. The format follows the standard LRFD format

$$\phi_R R_n \geq \sum_i \gamma_i Q_i \tag{2}$$

where  $\phi_R$  = resistance factor,  $R_n$  = nominal resistance,  $\gamma_i$  = load factor for load  $i$ , and  $Q_i$  = load component  $i$ . Considering the thermal loads for IABs, the basic limit state equation is expanded as

$$\phi_R R_n \geq \gamma_{DC} DC + \gamma_{DW} DW + \gamma_{LL} LL + \gamma_{IM} IM + \gamma_{IAB} IAB \tag{3}$$

where  $\gamma$  = load factors and IAB = thermal load that is load effects due to EH, TU, TG, CR and SH in an IAB. For simplicity, this study establishes a single load factor for IAB in the proposed supplementary LRFD limit state for the current AASHTO LRFD (2010) combinations.

The present study performed a reliability analysis to establish supplementary LRFD limit states exclusively for IABs. Previously developed nominal thermal load prediction models (Kim and Laman 2010b) were utilized in the reliability analysis models. Thermal load statistics were taken from an extensive Monte Carlo simulation study by Kim and Laman (2013). Other loads and resistance statistics were taken from the published literature. Based on the above described statistical models, this study established LRFD limit states for AASHTO LRFD Strength I, Service I and Service III limit states.

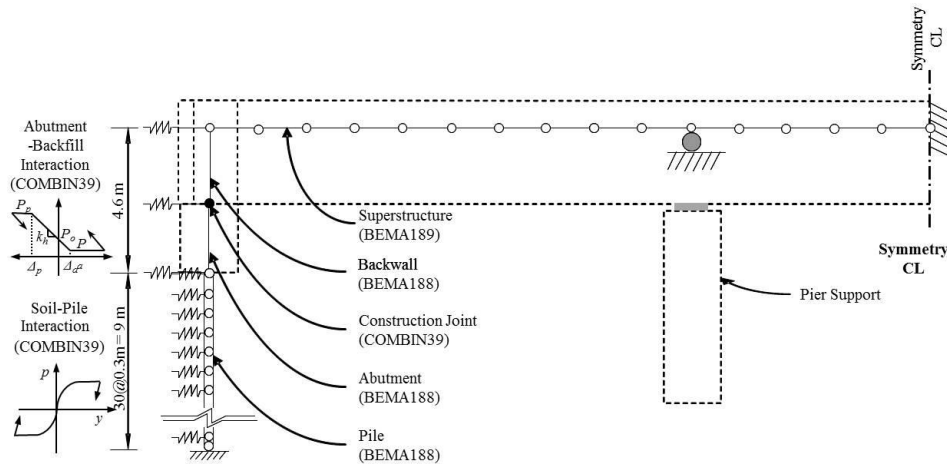


Fig. 2 2D nominal numerical model elevation

## 2. Statistics of loads and resistances

The load components of interest include dead load, live load and thermal load. Dead load is sustained and consists of bridge component self-weight (DC)-girders, deck slab, diaphragms and parapets-and wearing surface self-weight (DW). Other dead loads due to signs and utilities are not considered in this study. Bridge components are divided into cast-in-place and factory-made because of different uncertainties. Prestressed girders are assumed to be factory-made components and all other dead loads are cast-in-place components. IAB and jointed bridge dead load statistics can be considered as identical, therefore, statistics from the published literature (Nowak and Collins 2000) are utilized and presented in Table 2.

Live load statistics, which include traffic loads with vehicular impact for a 75-year bridge life, are also taken from published literature (Cheung and Li 2002, Nowak and Collins 2000) and are presented in Table 2. Other live loads, including wind load, snow load, etc. are not within the scope of this study. This study considers two live load models: (1) HL-93; and (2) HS-25 truck load + lane load. HL-93 load that is composed of HS20 truck load + lane load (9.34 kN/m) is a standard truck load used in AASHTO LRFD (2010). HS-25 truck load is 125% of HS20 truck load. In the HS-25 truck load + lane load, only truck load is increased to 125% compared to HL-93 and the lane load remains the same. If the HS-25 + lane load is used, the reliability indices of the existing bridge will decrease. However, the reliability indices will increase if it used in the design. The HS-25 truck + lane load model is also evaluated to consider future growth in vehicular live loads, however, the bias factor for this load equals  $1.10/1.25 = 0.88$  recognizing the HL-93 bias factor is 1.10. Truck impact, IM, is taken as a 33% (AASHTO LRFD 2010). Live loads are distributed to individual girders on the basis of the current approximate AASHTO LRFD girder distribution factors.

In IABs, EH, TU, TG, CR and SH are primary loadings that significantly influence bridge responses (Kim and Laman 2010a, b) and, therefore, must be considered in limit states. Because thermal loads result in complex, nonlinear behavior over a 75-year bridge life, a theoretical determination of a bridge response prediction model is not feasible. Utilizing the field measurement calibrated numerical models in Fig. 2 (Kim and Laman 2010a, 2013), a parametric

Table 3 Thermal load statistics (Kim and Laman 2011)

Load Component	Notation	Length m (ft)	Distribution	Bias Factor	COV
Tensile Stress	$f_{IAB-T}$	18.3 (60)	Normal	1.027	0.377
		61.0 (200)		0.387	3.440
		121.9 (400)		1.867	0.174
Compressive Stress	$f_{IAB-C}$	18.3 (60)	Normal	1.756	0.115
		61.0 (200)		1.259	0.204
		121.9 (400)		1.077	0.160
Bending Moment*	$M_{IAB}$	18.3 (60)	Normal	1.016	0.179
		61.0 (200)		1.850	0.319
		121.9 (400)		1.922	0.396

\*Negative moments at the mid-span

Table 4 Statistics for resistances (Kim and Laman 2011, Nowak and Collins 2000)

Material	Distribution	Bias Factor	COV
Prestressed Concrete (Bending)	Lognormal	1.05	0.075
$f_c' = 55.2$ MPa (8.0 ksi)	Lognormal	1.09	0.090
Modulus of Rupture ( $f_r$ ) (for $f_c' = 55.2$ MPa (8.0 ksi))	Lognormal	1.54	0.095

study was performed to establish nominal IAB response prediction models. The parametric study (Kim and Laman 2010b) considered five parameters: (1) thermal expansion coefficient, (2) bridge length, (3) backfill height, (4) backfill stiffness, and (5) pile soil stiffness. Based on the calibrated numerical models and soil and concrete material statistics, Kim and Laman (2013) performed Monte Carlo simulations to establish a 75-year IAB response database. The established thermal load statistics for the above described loads are summarized in Table 3.

Statistics of bridge structure resistance from published literature (Nowak and Collins 2000, Nowak and Szerszen 2003, Tabsh and Nowak 1991, Hueste *et al.* 2004) that are the basis of the current AASHTO LRFD are utilized and described in Table 4.

### 3. Reliability analysis of AASHTO LRFD limit state

Reliability analyses of AASHTO LRFD (2010) limit states have been performed to determine whether the additional IAB thermal loads reduce structure safety. Many reliability analysis examples for bridges have been done by other researchers (Stewart 2001, Hamutcuoglu and Scott 2009). A reliability analysis determines the safety level of a structure in terms of a reliability index ( $\beta$ ) and is computed here for two loading cases: (1) a bridge without thermal load; and (2) a bridge with thermal load. For the reliability analysis of this study, loads and resistances are considered to be uncorrelated.

AASHTO LRFD limit states, with the same objectives and load and resistance definitions, have been considered in the reliability analysis for the present study while AASHTO load factors for TU, TG, EH, CR and SH are not applicable to the proposed new LRFD limit state. Thermal loading is added to AASHTO Service I, Service III and Strength I limit state. The service limit

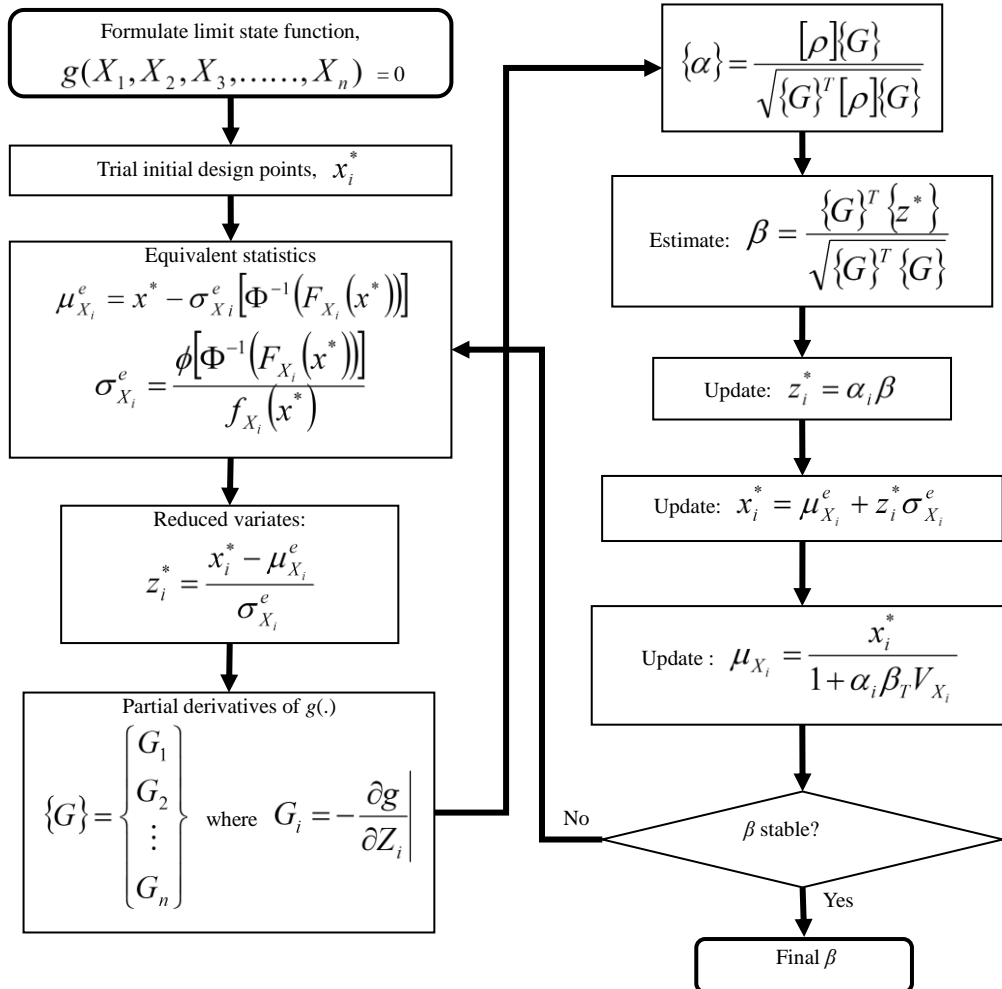


Fig. 3 Reliability analysis procedure

states are intended to provide a limit for deflection, cracking, vibration and gradual deterioration based on user's comfort, aesthetics or cost. The strength limit state provides a minimum level of safety based on strength capacity. The objective of the Service I limit state is to provide for the normal operation of a bridge without compressive failure. The Service III limit state limits tension cracking of prestressed concrete superstructures under normal operation. As discussed in AASHTO LRFD (2010) commentary (C3.4.1), Service III limit state event occurs about once per day for single traffic lane bridges, once per year for two traffic lane bridges and less often for bridges with more than two traffic lanes.

The Rackwitz-Fiessler procedure (Rackwitz and Fiessler 1978) can be employed to compute reliability indices for each of the limit states. Rackwitz-Fiessler is based on variable statistics and distribution types of all related variables in a limit state function.

### 3.1 Service I limit state

The AASHTO LRFD Service I limit state (AASHTO LRFD 5.9.4.2.1) is a limit state relating to the normal operational use of a bridge. Therefore, all load factors for considered loads are taken equal to 1.0. The limit state for the Service I limit state at the top fiber of the prestressed concrete girder is

$$\phi_R f_n \geq \sum_i \gamma_i f_i = 1.0 f_{DC1} + 1.0 f_{DC2} + 1.0 f_{DW} + 1.0 f_{LL+IM} \tag{4}$$

where  $\phi_R$  = resistance factor,  $f_n$  = nominal compressive stress,  $f_{DC1}$  = compressive stress due to factory-made DC,  $f_{DC2}$  = compressive stress due to cast-in-place DC,  $f_{DW}$  = compressive stress due to DW, and  $f_{LL+IM}$  = compressive stress due to LL+IM.

AASHTO specifies two compressive stress limits in terms of concrete compressive stress ( $f_c'$ ): (1)  $0.45 f_c'$  for the sum of effective prestress and permanent loads; and (2)  $0.6 f_c'$  for the sum of effective prestress, permanent loads, and transient loads. The required resistance can be obtained from the summation of all load effects. Therefore, the stress limit specified by AASHTO LRFD was adopted as the nominal resistance ( $f_n$ ) of the structure. Considering the additional compressive stress due to thermal load ( $f_{IAB}$ ), the Service I limit state for permanent loads is

$$\phi_R f_n = 0.45 f_c' \geq 1.0 f_{DC1} + 1.0 f_{DC2} + 1.0 f_{DW} + 1.0 f_{IAB} \tag{5}$$

For all dead loads and live loads, the Service I limit state is:

$$\phi_R f_n = 0.6 f_c' \geq 1.0 f_{DC1} + 1.0 f_{DC2} + 1.0 f_{DW} + 1.0 f_{LL+IM} + 1.0 f_{IAB} \tag{6}$$

Therefore, the limit state function,  $g(\cdot)$  for permanent loads is:

$$g(\cdot) = 0.6 f_c' - (f_{DC1} + f_{DC2} + f_{DW} + f_{LL+IM} + f_{IAB}) = 0 \tag{7}$$

Reliability indices ( $\beta$ ) were computed for both Service I limit states and are presented in Figs. 4 and 5. Based on Eqs. (6) and (7),  $\beta_s$  for the Service I limit state with thermal load ('IA bridge' in Figs. 4 and 5) were computed. For comparison purposes,  $\beta$  for the Service I limit state without thermal load (without  $f_{IAB}$  in Eqs. (6) and (7)) have also been computed. In addition, two live load models were considered for all loading cases (Fig. 5). The transition of design live load from HL-93 load to HS-25 + lane load (bias factor decreases 25% and lane load increases 25%) causes  $\beta$  to decrease approximately 29%.

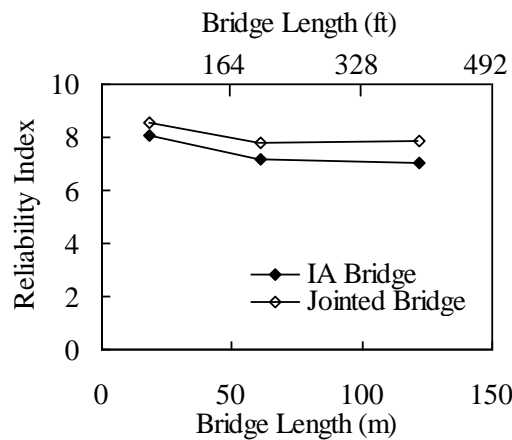


Fig. 4 Service I limit state reliability indices for permanent loads

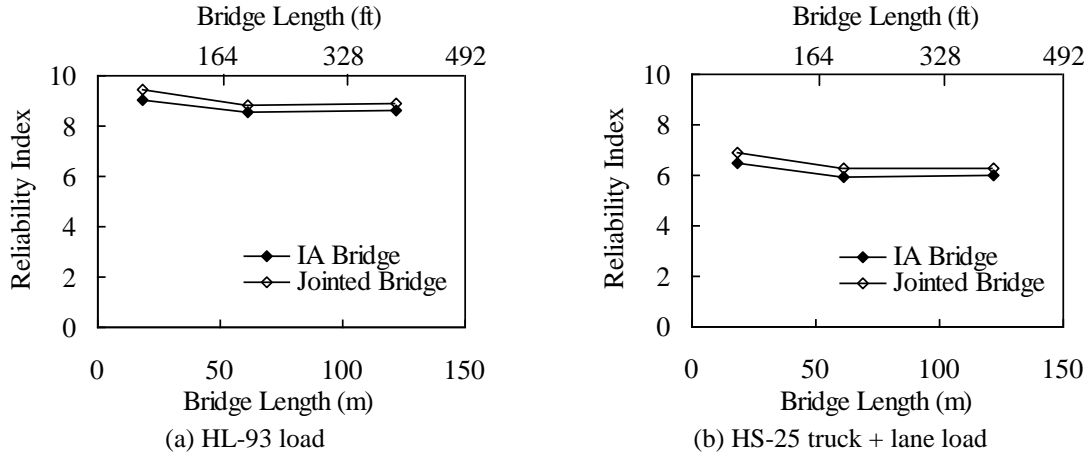


Fig. 5 Service I limit state reliability indices for all loads

For Service I permanent loads (see Fig. 4),  $f_{IAB}$  significantly influences bridge reliability. For permanent loads,  $\beta$  for IABs ranges between 7.0 and 8.1 and  $\beta$  for jointed bridges ranges between 7.8 and 8.5.  $f_{IAB}$  reduces  $\beta$  by approximately 8.1% for the Service I permanent load limit state.

Considering the Service I limit state (see Fig. 5), the influence of  $f_{IAB}$  is relatively small on bridge reliability. For the HL-93 load,  $\beta$  for IABs ranges from 8.5 to 9.0 and  $\beta$  for jointed bridges ranges from 8.8 to 9.4. The  $f_{IAB}$  reduces  $\beta$  by approximately 3.5% for Service I under the HL-93 load. Under the HS-25 truck + lane load,  $\beta$  for IABs ranges from 5.8 to 6.5 and for jointed bridges ranges from 6.3 to 6.9. The  $f_{IAB}$  reduced  $\beta$  by approximately 5.1% for Service I with HS-25 truck + lane load. The computed reliability indices correspond to relatively low probabilities of failures; less than  $4.8E-13$  under HL-93 and  $7.4E-10$  under HS-25 truck + lane load, however,  $f_{IAB}$  does influence the overall Service I limit state and bridge reliability.

### 3.2 Service III limit state

The AASHTO LRFD Service III limit state (AASHTO LRFD 5.9.4.2.2) evaluates tension in prestressed concrete girder bridges for crack control. The limit state for Service III limit state is

$$\phi_R f_n \geq \sum_i \gamma_i f_i = 1.0 f_{DC1} + 1.0 f_{DC2} + 1.0 f_{DW} + 0.8 f_{LL+IM} \quad (9)$$

This limit state adopts load factors equal to 1.0 for all loads except vehicular live loads. As discussed in AASHTO LRFD, the live load load factor ( $\gamma_{LL+IM} = 0.8$ ) in the Service III limit state has been selected to represent an occurrence of prestressed concrete girder crack opening frequency.

AASHTO LRFD specifies a tensile stress limit of  $0.5\sqrt{f'_c}$  (MPa) ( $0.19\sqrt{f'_c}$  (ksi)), which is a lower-bound value for the tensile strength (Hueste *et al.* 2004). Thus, the bias factor for the modulus of rupture (1.54) from published literature (Hueste *et al.* 2004) is significantly larger than 1.0 as presented in Table 4. The applied nominal stress can be obtained by computing a resultant stress due to the expected loads, however, this resultant stress is limited by the tensile stress limit of  $0.5\sqrt{f'_c}$  (MPa) ( $0.19\sqrt{f'_c}$  (ksi)). The AASHTO tensile stress limit, therefore, is the nominal resistance ( $f_n$ ) in a reliability analysis. Considering the additional tensile stress due to thermal loads

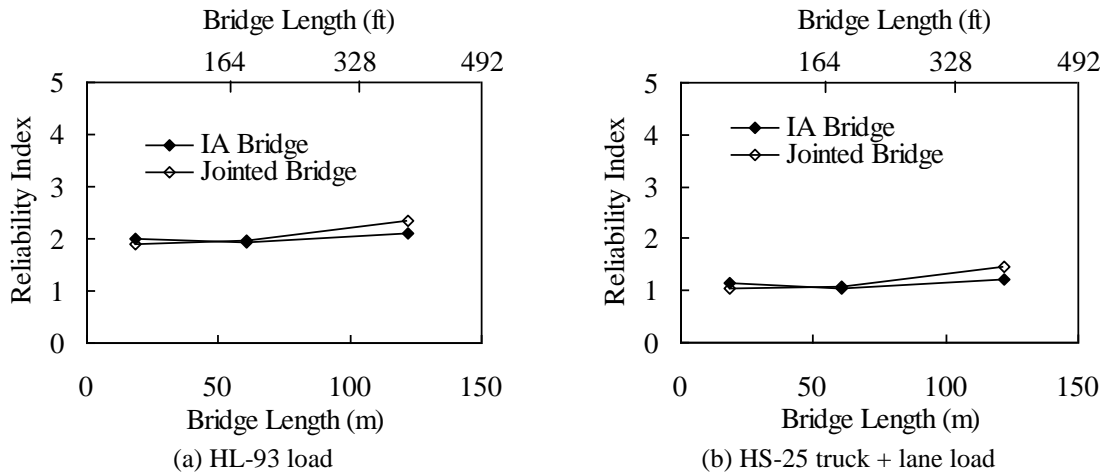


Fig. 6 Load factors for service III limit state

( $f_{IAB}$ ), the limit state of Service III is

$$\begin{aligned} \phi_R f_n = 0.5\sqrt{f'_c} &\geq 1.0 f_{DC} + 1.0 f_{DW} + 0.8 f_{LL+IM} + 1.0 f_{IAB} \text{ (MPa)} \\ \phi_R f_n = 0.19\sqrt{f'_c} &(\geq 1.0 f_{DC} + 1.0 f_{DW} + 0.8 f_{LL+IM} + 1.0 f_{IAB} \text{ (ksi)}) \end{aligned} \quad (10)$$

Therefore, the limit state function,  $g(\cdot)$  for Service III is

$$\begin{aligned} g(\cdot) &= 0.5\sqrt{f'_c} - (f_{DC} + f_{DW} + 0.8 f_{LL+IM} + f_{IAB}) \text{ (MPa)} \\ g(\cdot) &= 0.19\sqrt{f'_c} - (f_{DC} + f_{DW} + 0.8 f_{LL+IM} + f_{IAB}) \text{ (ksi)} \end{aligned} \quad (11)$$

Reliability indices ( $\beta$ ) are computed for the Service III limit state and are presented in Fig. 6. Based on Eq. (11),  $\beta$  for the Service III limit state with thermal load ('IA bridge' in Fig. 6) is computed. For comparison purposes,  $\beta$  for the Service III limit state without thermal load (without  $f_{IAB}$  in Eq. (11)) are also computed. In addition, live load models of HL-93 and HS25 truck + lane load were considered.

The  $\beta$  for bridges under the HL-93 load is approximately 2.0. Similarly,  $\beta$  under the HS-25+lane load is approximately 1.0. The change in the nominal design live load model from HL-93 to HS-25+lane load causes  $\beta$  to decrease by approximately 43%.

The influence of  $f_{IAB}$  on bridge reliability under the Service III limit state is small but not insignificant for the considered bridge lengths. Under the HL-93 load,  $\beta$  for IABs ranges from 1.9 to 2.1 and  $\beta$  for jointed bridges ranges from 1.9 and 2.3. The inclusion of  $f_{IAB}$  reduces  $\beta$  by approximately 5.4% for  $L = 60.9$  and  $121.9$  m (200 and 400 ft). However,  $\beta_s$  for  $L = 18.3$  m (60 ft) increased 6.2% because bridges with  $L = 18.3$  m (60 ft) experience no tensile stress due to  $f_{IAB}$  but always compression. The influence  $f_{IAB}$  can be expected to be much more significant and detrimental for longer spans because the influence continuously increases (Fig. 6).

### 3.3 Strength I limit state

The AASHTO LRFD Strength I limit state is a limit state for investigating strength demand

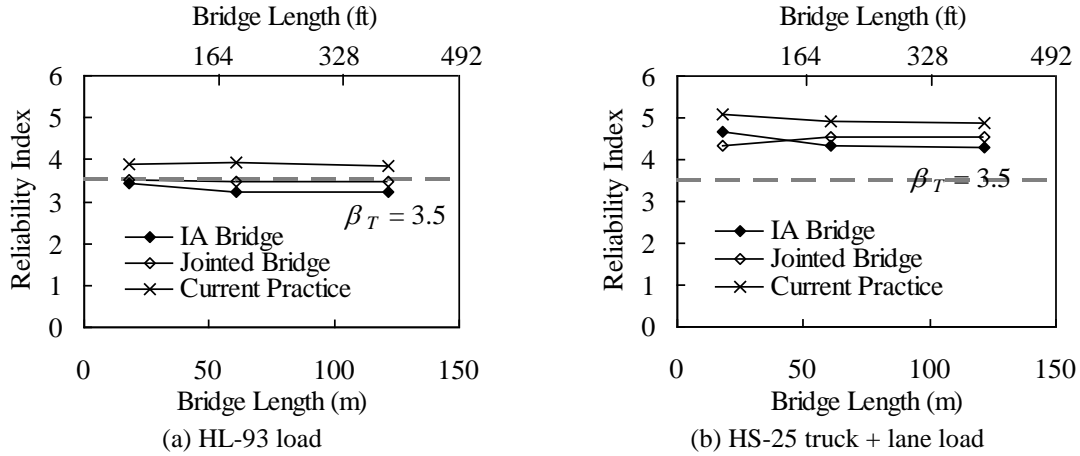


Fig. 7 Strength I limit state reliability indices

relating to the normal vehicular use of the bridge without wind. The general strength limit state is formulated in Eq. (1). Relative to bending moment, the limit state for Strength I limit state is

$$\phi_R M_n \geq 1.25M_{DC1} + 1.25M_{DC2} + 1.5M_{DW} + 1.75M_{LL+IM} \quad (12)$$

where,  $M_{DC1}$  = moment due to factory-made DC,  $M_{DC2}$  = moment due to cast-in-place DC,  $M_{DW}$  = moment due to DW, and  $M_{LL+IM}$  = moment due to LL+IM.

The load factor for thermal loading ( $\gamma_{IAB}$ ) is determined by

$$\gamma_{IAB} = \lambda_{IAB}(1 + \eta \text{COV}_{IAB}) \quad (13)$$

where,  $\lambda_{IAB}$  = bias factor for thermal loading,  $\eta$  = constant determined by the target reliability exceedance probability ( $\eta = 2.0$  for current AASHTO by Nowak 1995), and  $\text{COV}_{IAB}$  = coefficient of variation of thermal loading.

In the strength limit state considered here, resistance is measured in terms of flexural strength. The nominal flexural strength ( $M_n$ ) is derived from the design limit state as

$$M_n = \frac{1}{\phi_R} [1.25M_{DC1} + 1.25M_{DC2} + 1.5M_{DW} + 1.75M_{LL+IM}] \quad (14)$$

where,  $\phi_R$  = resistance factor (= 1.0 for bending in accordance with AASHTO LRFD). Considering the additional bending moment due to thermal load ( $M_{IAB}$ ), a limit state function for Strength I limit state is modified as:

$$g(\cdot) = M_n - (M_{DC1} + M_{DC2} + M_{DW} + M_{LL+IM} + M_{IAB}) = 0 \quad (15)$$

A target reliability of 3.5 was adopted for the Strength I limit state for consistency with current AASHTO LRFD.

Based on Eq. (15) reliability indices ( $\beta$ ) were computed for Strength I limit state and are presented in Fig. 7. For comparison purposes,  $\beta$  was computed without the inclusion of thermal effects (without  $M_{IAB}$  in Eq. (15)). In addition,  $\beta$  corresponding to current IAB design practice ( $M_n$  in Eq. (15) without  $M_{IAB}$ ) was computed to demonstrate the effect of design without considering thermal effects. Both live load models of HL-93 and HS25 truck + lane load were demonstrated.

$\beta$  of IA bridges in Fig. 7 decrease as bridge length increases by 5.9% and 0.6% for HL-93 loads

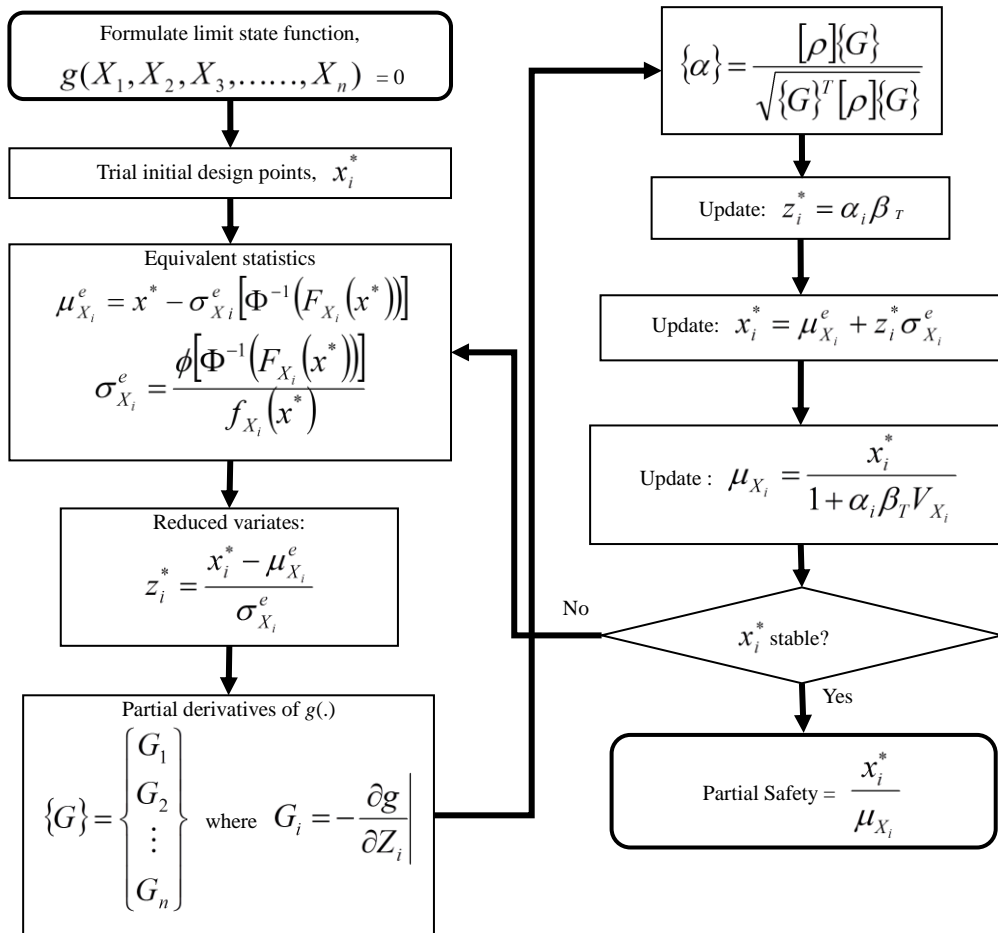


Fig. 8 Partial safety factor calibration procedure

and HS-25 truck + lane loads, respectively. For IABs,  $\beta$  average with thermal effects included is 3.2 for HL-93 and 4.4 for HS-25 truck + lane load.  $\beta$  average for current practice is 3.9 for HL-93 and 5.0 for HS-25 truck + lane load. Therefore, the load factors for thermal effects are re-computed to obtain a constant reliability index over bridge length and to be consistent with the current AASHTO LRFD.

#### 4. Calibration of load and resistance factors

Load and resistance factors were determined for the Strength I limit state through reliability analyses for AASHTO limit states. Using the partial safety factor calibration procedure (Nowak and Collins 2000) presented in Fig. 8, partial safety factors to achieve a target reliability index  $\beta_T = 3.5$  were computed. The calibration procedure is an iterative computational procedure that is similar to that presented in Fig. 3.

Table 5 Partial safety factors for  $\beta_T = 3.5$  (HL-93 load)

Limit State	Length $m$ (ft)	$R$	$\gamma_{DC1}$	$\gamma_{DC2}$	$\gamma_{DW}$	$\gamma_{LL+IM}$	$\gamma_{IAB}$
Strength I	18.3 (60)	0.85	1.10	1.05	1.20	1.60	1.00
	61.0 (200)	0.85	1.15	1.05	1.20	1.50	1.50
	121.9 (400)	0.85	1.15	1.05	1.20	1.50	1.50

Table 6 Partial safety factors for  $\beta_T = 3.5$  (HS-25 truck + lane load)

Limit State	Length $m$ (ft)	$R$	$\gamma_{DC1}$	$\gamma_{DC2}$	$\gamma_{DW}$	$\gamma_{LL+IM}$	$\gamma_{IAB}$
Strength I	18.3 (60)	0.85	1.10	1.05	1.20	1.60	1.00
	61.0 (200)	0.85	1.15	1.05	1.15	1.55	1.30
	121.9 (400)	0.85	1.15	1.05	1.15	1.55	1.55

After establishing a limit state function,  $g(\cdot) = 0$ , including all loads and resistance components of interest in this limit state, the initial design point ( $x_i^*$ ) is assumed to start the analysis. Equivalent normal variables ( $\mu_{X_i}^e, \sigma_{X_i}^e$ ) are computed, and these variables are transferred to the reduced variates ( $z_i^*$ ) corresponding to the design point ( $x_i^*$ ). Partial derivatives of  $g(\cdot) = 0$  and the directional cosine vector are determined at the design point. Using the target reliability index, an updated design point is computed in reduced variates. The design point in the original coordinates is updated based on this updated design point in reduced variates. This procedure is iterated until a constant partial safety factor is obtained. Using the procedure presented in Fig. 8, partial safety factors are determined (Tables 5 and 6) to achieve the target reliability index ( $\beta_T = 3.5$ ). As observed from Tables 5 and 6, load and resistance factors are a function of bridge length. However, establishing load and resistance factors as a function of length is not practical. Therefore, this study investigated thermal load factors with respect to different resistance factors to achieve the target reliability index.

A resistance factor,  $\phi_R$  equal to 1.0 is specified by AASHTO LRFD for prestressed concrete girders subjected to bending moment. For a compression-controlled section,  $\phi_R$  equals 0.75 to prevent brittle failure. For those sections subjected to axial force with flexure,  $\phi_R$  is calculated as 0.75 (compression-controlled)  $\times$  1.0 (prestressed girder bending) = 0.75 (AASHTO LRFD C5.5.4.2.1). However, short-to-medium span IAB prestressed concrete girders are typically not compression controlled sections, but tension-controlled because compressive stress is relatively small compared to bending as investigated in the Service I limit state. Because the current AASHTO LRFD does not specify a resistance factor for the condition of bending moment + compression force, the present study, investigates  $\gamma_{IAB}$  with respect to  $\phi_R = 0.85$  to 1.0.

For comparison purposes, abutment rotational stiffness was evaluated at two extremes – no stiffness and infinite stiffness. Actual IAB abutment rotational stiffness falls somewhere between simple and fixed because the backwall and deck are integrally cast around the abutments. However, the construction joint between backwall and abutment and weak-axis oriented supporting piles allow structure rotation (Kim and Laman 2012). The rotational stiffness of an abutment is difficult to predict because it is related to the superstructure and substructure dimensions and shapes, pile rotational capacity, soil properties, and load history. Therefore, the present study analyzes the bridge reliability based on both simple support and fixed end support as presented in Fig. 9. In order to incorporate the dead load supported at the abutment, simply supported conditions are evaluated, recognizing a typical construction sequence.

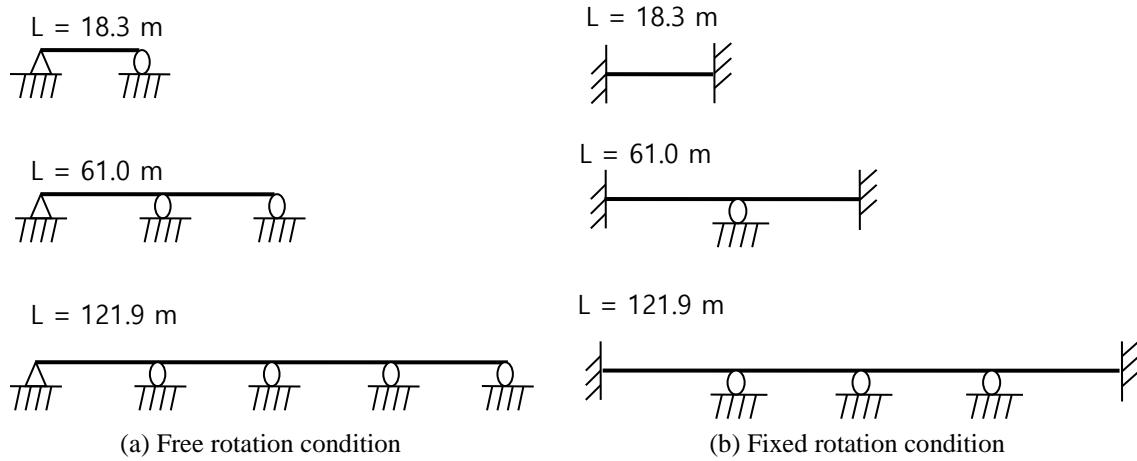
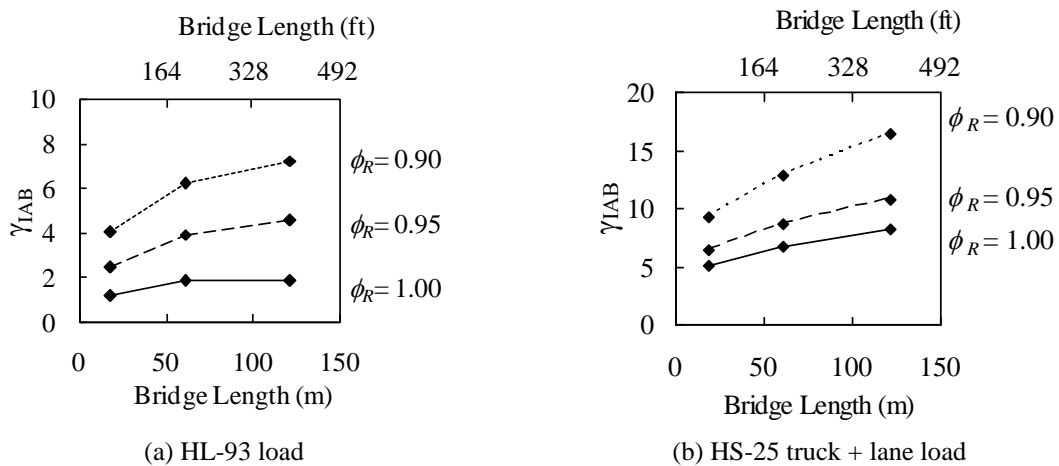


Fig. 9 Analysis rotation conditions



Note:  $\gamma_{DC} = 1.25$ ,  $\gamma_{DW} = 1.5$ ,  $\gamma_{LL+IM} = 1.75$

Fig. 10 Load factors for thermal loads (simple support)

#### 4.1 Free rotation abutment condition

Based on a free rotation abutment condition assumption, a reliability analysis was performed to determine  $\gamma_{IAB}$  for values of  $\phi_R = 0.85, 0.90, 0.95,$  and  $1.0$  for Strength I limit state. For consistency with AASHTO LRFD, DC, DW and LL + IM load factors correspond with the AASHTO LRFD Strength I limit state. Both HL-93 and HS-25 truck + lane loads were applied to establish partial load factors for each live load model. The partial load factor  $\gamma_{IAB}$ , with  $\phi_R = 0.85, 0.90, 0.95,$  and  $1.0$  was determined for each bridge length as presented in Fig. 10. The magnitude of  $\gamma_{IAB}$  for HS-25 truck load + lane load changes significantly as bridge length increases. Based on the reliability analysis results,  $\phi_R = 1.00$  and  $\gamma_{IAB} = 1.15$  for HL-93 loads provides a constant level of safety. Fig. 11 presents reliability indices of various combinations of  $\phi_R$  and  $\gamma_{IAB}$ .

Based on the final, proposed resistance and load factors ( $\phi_R = 1.00$  and  $\gamma_{IAB} = 1.15$ ), a reliability

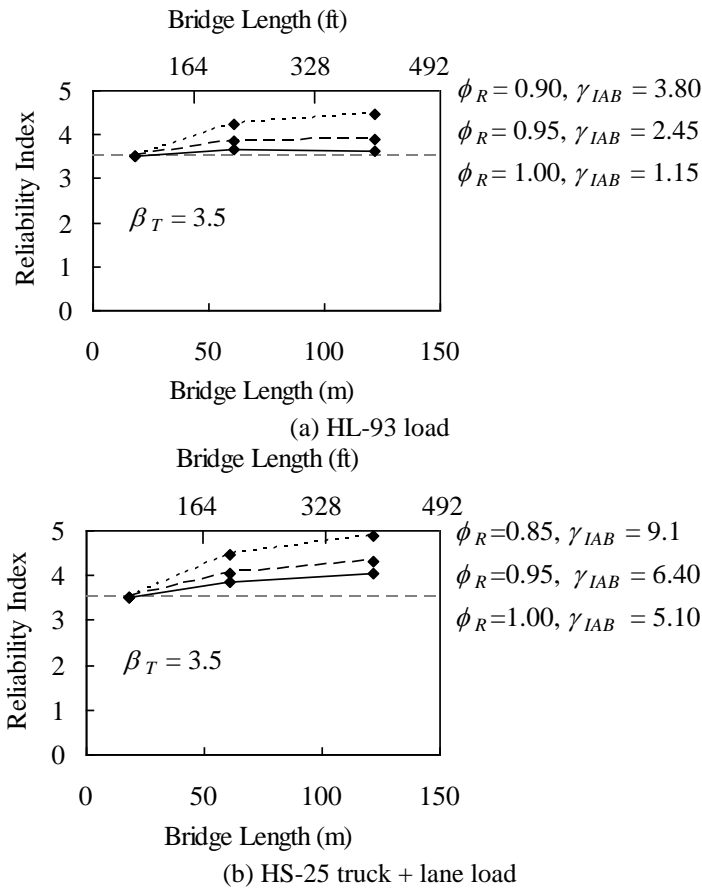


Fig. 11 Proposed load and resistance factors (simple support)

analysis was performed for a full range of dead load over total load ( $DC/(DC+LL)$ ), ranging from 0.0 to 1.0. In addition, thermal load is a function of bridge length and abutment stiffness. The ratio of thermal to dead load ( $IAB/DC$ ) was evaluated for both 0.05 and 0.15. Fig. 12 presents  $\beta$  with respect to  $DC/(DC+LL)$  for both ratios. In the analysis,  $DW/DC = 12.5\%$  was assumed. For the practical load ratio ranges between 0.3 and 0.9 (Nowak and Szerszen 2003),  $\beta$  varies from 2.9 to 3.8.

#### 4.2 Fixed rotation abutment condition

Based on a fixed rotation abutment condition assumption, a reliability analysis was performed to determine  $\gamma_{IAB}$  for values of  $i = 0.85, 0.90, 0.95,$  and  $1.0$  for Strength I limit state. For consistency with AASHTO LRFD, DC, DW and LL + IM load factors correspond with the AASHTO LRFD Strength I limit state. Both HL-93 and HS-25 truck + lane loads were applied to establish partial load factors for each live load model.

Current IAB design practice was investigated in terms of reliability index. Fig. 13 presents  $\beta$  for both boundary conditions: (1) an IAB girder designed as simply supported (without IAB load), however, the actual rotational condition is partially restrained (DSBF), and (2) an IAB girder

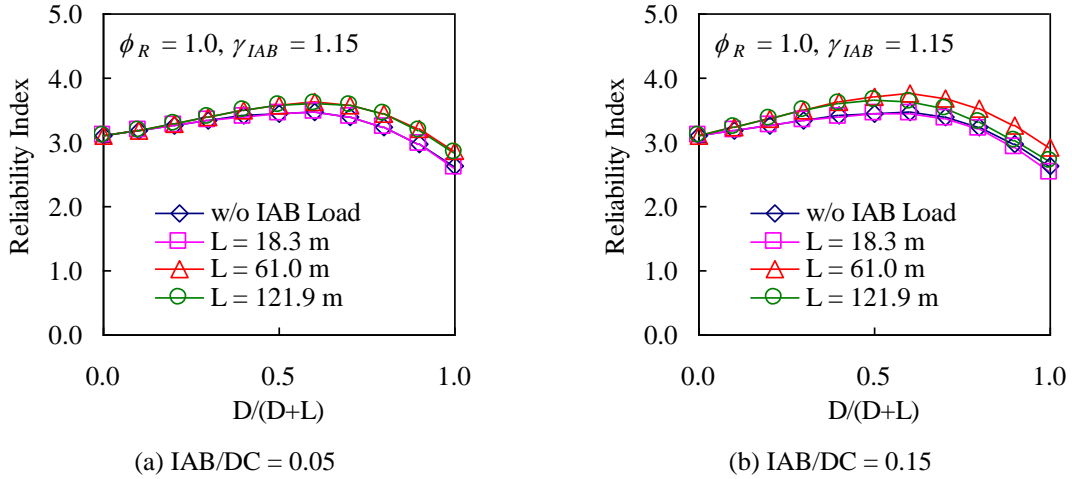


Fig. 12 Reliability indices for ratios of IAB to DC

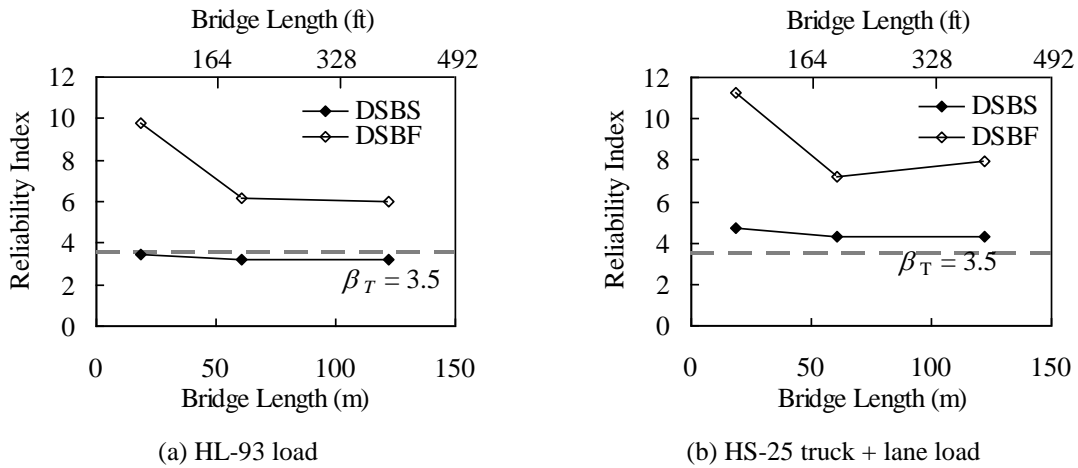


Fig. 13 Reliability indices for IABs with respect to boundary condition

designed as simply supported and the actual boundary is simply-supported (DSBS). Fig. 13 presents  $\beta$  as a function of bridge length for both DSBF and DSBS. A fixed rotational restraint assumption leads to a much greater  $\beta$  than either the target reliability or that for DSBS. Therefore, results indicate that the current IAB design practice is conservative compared to AASHTO LRFD conventional bridge design because the  $\beta$  s of IABs range between 3.5 and 12.

Determined load factors with respect to  $\phi_R = 0.85$  to 1.0 to achieve the target reliability,  $\beta = 3.5$  for each bridge are presented in Fig. 14. As  $\phi_R$  decreases,  $\gamma_{IAB}$  increases. This inverse relationship is more pronounced as bridge length increases.  $\phi_R = 1.00$  and  $\gamma_{IAB} = 1.15$  for HL-93 loads provide a constant level of safety. Other  $\phi_R$  values may lead to more conservative bridge design, therefore,  $\phi_R = 1.00$  and  $\gamma_{IAB} = 1.15$  is proposed for IAB design consistent with the current AASHTO LRFD. Fig. 15 presents reliability indices based on the proposed load and resistance factors and comparison to different  $\phi$ s and  $\gamma_{IAB}$  s.

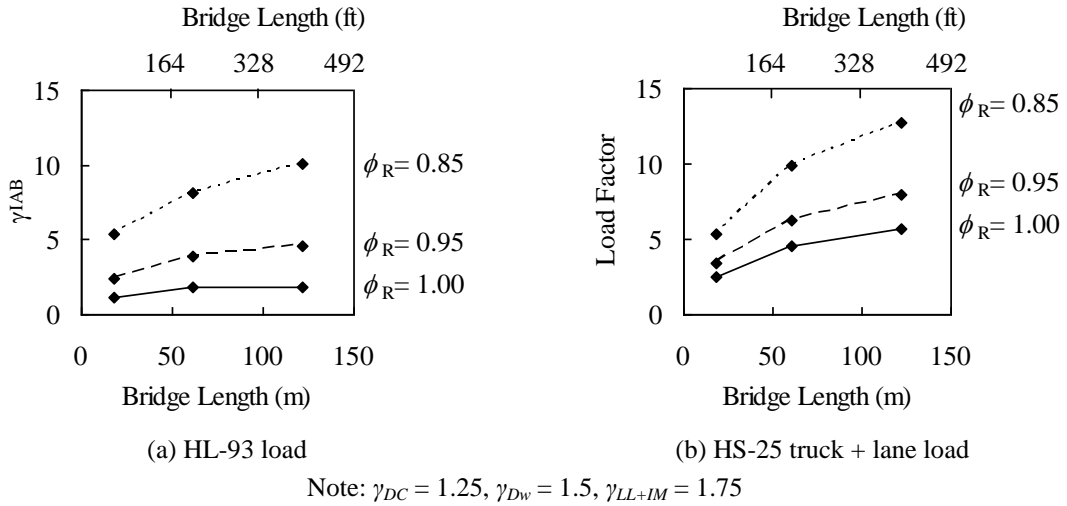


Fig. 14 Load factors for thermal loads (fix end support)

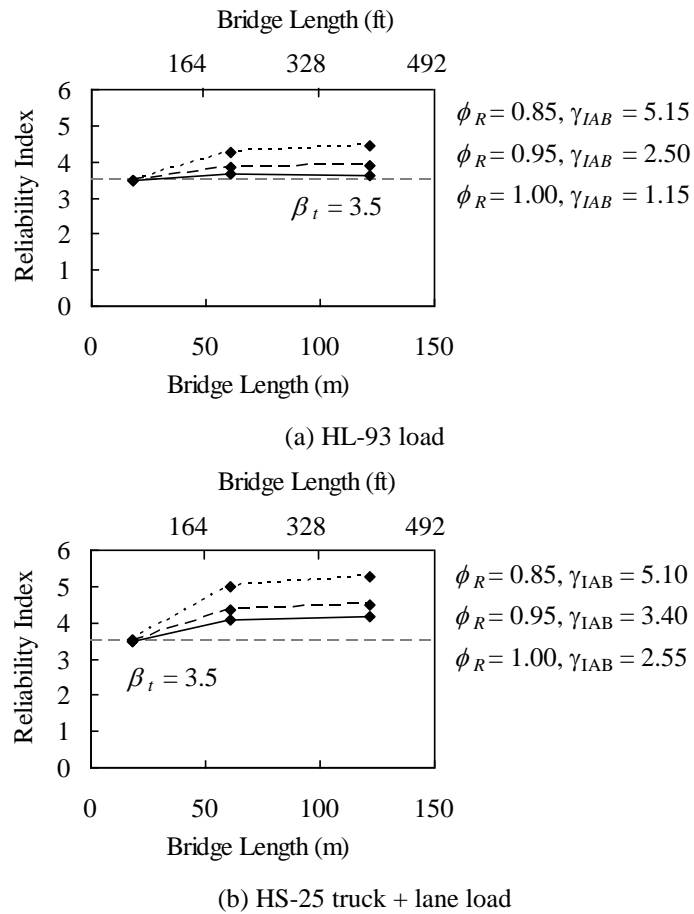


Fig. 15 Proposed load and resistance factors (fixed end support)

## 5. Conclusions

Based on the previously established thermal load response statistics, reliability analyses were performed to determine the limit states for short to medium length, four, prestressed concrete girder IABs. An IAB has different boundary and loading conditions compared to a jointed bridge and the load effects of EH, TU, TG, CR and SH are, therefore, primary loading rather than secondary. This study established new, limit states specific to IAB prestressed concrete girder design. The AASHTO LRFD Service I, Service III and Strength I limit state were selected as limit state functions. For live loads, both live load models of HL-93 loads and HS-25 truck + lane loads were considered in the reliability analyses. Simple support and fixed end support conditions were also considered in the reliability analysis for Strength I limit state.

Established limit states for IABs are:

(1) Service I (permanent loads only)

$$1.0 f_{DC} + 1.0 f_{DW} + 1.0 f_{IAB} \leq 0.45 f_c' \quad (16)$$

(2) Service I (all dead loads and live loads)

$$1.0 f_{DC} + 1.0 f_{DW} + 1.0 f_{LL+IM} + 1.0 f_{IAB} \leq 0.6 f_c' \quad (17)$$

(3) Service III

$$1.0 f_{DC} + 1.0 f_{DW} + 0.8 f_{LL+IM} + 1.0 f_{IAB} \leq 0.5\sqrt{f_c'} \text{ (MPa)} \quad (18)$$

$$1.0 f_{DC} + 1.0 f_{DW} + 0.8 f_{LL+IM} + 1.0 f_{IAB} \leq 0.19\sqrt{f_c'} \text{ (ksi)}$$

(4) Strength I

$$\phi_R M_n = 1.25M_{DC} + 1.50M_{DW} + 1.75M_{LL+IM} + 1.15M_{IAB} \quad (\phi_R = 1.0) \quad (19)$$

## Acknowledgements

This research was supported by Basic Science Research Program through the National Research Foundation of Korea (NRF) funded by the Ministry of Education, Science and Technology (2012R1A1A1044378).

## References

- American Association of State Highway and Transportation Officials (AASHTO LRFD) (2010), *AASHTO LRFD bridge design specifications*, Washington, D.C.
- Arockiasamy, M., Butrieng, N. and Sivakumar, M. (2004), "State-of-the-art of integral abutment bridges: design and practice", *J. Bridge Eng.*, **9**(5), 497-506.
- Cheung, M.S. and Li, W.C. (2002), "Reliability assessment in highway bridge design", *Can. J. Civil Eng.*, **29**, 799-805.
- Hamutcuoglu, O. and Scott, M.H. (2009), "Finite element reliability analysis of bridge girders considering moment-shear interaction", *Struct. Saf.*, **31**(5), 356-362.
- Hueste, M.B.D., Chompreda, P., Trejo, D., Cline, D.B.H. and Keating, P.B. (2004), "Mechanical properties of high-strength concrete for prestressed members", *ACI Struct. J.*, **101**(S45), 457-465.

- Kim, W. and Laman, J.A. (2010a), "Long-term numerical analysis of integral abutment bridges", *Eng. Struct.*, **32**(8), 2247-2257.
- Kim, W. and Laman, J.A. (2010b), "Integral abutment bridge response under thermal loading", *Eng. Struct.*, **32**(6), 1495-1508.
- Kim, W. and Laman, J.A. (2012), "7-year field monitoring of four integral abutment bridges", *J. Perform. Constr. Facil.*, **26**(1), 54-64.
- Kim, W. and Laman, J.A. (2013), "Integral abutment bridge behavior under uncertain thermal and time-dependent load", *Struct. Eng. Mech.*, **46**(1), 53-73.
- Nowak, A.S. (1995), "Calibration of LRFD Bridge Code", *ASCE J. Struct. Eng.*, **121**(8), 1245-1251.
- Nowak, A.S. and Collins, K.R. (2000) *Reliability of Structures*, ISBN 0-07-048163-6, CRC, US.
- Nowak, A.S. and Szerszen, M.M. (2003), "calibration of design code for buildings (ACI 318): part 1-statistical models for resistance", *ACI Struct. J.*, **100**(3), 377-382.
- Rackwitz, R. and Fiessler, B. (1978), "Structural reliability under combined random load sequences", *Comput. Struct.*, **9**, 489-494.
- Stewart, M.G. (2001), "Reliability-based assessment of ageing bridges using risk ranking and life cycle cost decision analyses", *Reliab. Eng. Syst. Saf.*, **74**(3), 263-273.
- Tabsh, S.W. and Nowak, A.S. (1991), "Reliability of highway girder bridges", *ASCE J. Struct. Eng.*, **117**(8), 2373-2388.